Structurally Defined 3D Nanographene Assemblies via Bottom-Up Chemical Synthesis for Highly Efficient Lithium Storage

Hung-Ju Yen, Hsinhan Tsai, Ming Zhou, Edward F. Holby, Samrat Choudhury, Aiping Chen, Lyudmyla Adamska, Sergei Tretiak, Timothy Sanchez, Srinivas Iyer, Hanguang Zhang, Lingxiang Zhu, Haiqing Lin, Liming Dai, Gang Wu, and Hsing-Lin Wang**

New electrode materials with faster electron transport, larger ion storage capacity, and more efficient Li ion diffusion are of particular interest to next generation lithium ion batteries (LIBs). These properties are crucial for meeting the rapidly increasing demands of high-power and high energy densities for energy storage. One of recent efforts has been devoted to developing advanced anode materials with increased number of lithiation sites and faster Li diffusion rates.[1] Among studied advanced materials, although silicon has been shown to have a high theoretical gravimetric capacity of ≈4200 mAh g^{-1} compared to graphite's 372 mAh g^{-1}, they suffer from rapid degradation with each cycle due to electrode volume expansion of ≈400% during lithiation putting strain on the material.[2] Alternatively, graphene, a 2D honeycomb lattice and simply one atomic layer of graphite has emerged as one of the most exciting materials mainly because of its extraordinary thermal, mechanical, and electrical properties. Graphene holds enormous potential for widespread applications, such as nanoscale electronic devices, composite materials, sensors, solar cells, hydrogen storage, and electrodes for LIBs.[3] In particular, its high electron conductivity, large specific surface area (up to 2648 m^2 g^{-1}), and broad electrochemical potential window hold great promise for this material to be used as an advanced anode in LIBs for portable electronics and electric vehicles.[1f,4] In addition, due to the fact that Li ions can adsorb on both sides of the atomic-thick carbon sheet, graphene anodes exhibited a substantially improved specific charge capacity over graphite (theoretical capacity of 372 mAh g^{-1}) that can only intercalate one Li atom per six carbon atoms (LiC_6).[5] Moreover, the single-layer graphene is capable of facilitating Li diffusion with a lower barrier than that of graphite interlayers.[6] In graphene family, graphene oxide (GO) is the most important precursor to prepare graphene materials via a reduction reaction. Recent studies revealed that structural modification of GO through hydrazine reduction, high temperature pyrolysis, and electron beam irradiation has led to an increased charge capacity.[7] In addition, nitrogen/boron doping[8] and phosphorous/nitrogen dual-doped porous graphene[9] are also used as a LIB anode to achieve high capacity. However, these previous approaches to achieve higher capacity (up to 780 mAh g^{-1}) by increasing *d*-spacing are lack of structural control and detailed characterization. The hypothesis of increasing charge capacity through increasing *d*-spacing is not experimentally validated. Precise molecular control to clearly elucidate the correlation between structure and properties is required by using structurally defined graphene assemblies via bottom-up chemical synthesis.[6,10] Such a well-controlled system would aid in designing optimal graphene anodes with ideal geometrical and electronic structures for maximum capacity. Moreover, another major problem with current graphene-based anodes is that they experience a significant irreversible capacity loss (>50%) during charging/discharging cycles, due to restacking of graphene layers.[1h,4b,11] To mitigate

Dr. H.-J. Yen, H. Tsai, Dr. M. Zhou, Dr. H.-L. Wang
Physical Chemistry and Applied Spectroscopy (C-PCS)
Chemistry Division
Los Alamos National Laboratory
Los Alamos, NM 87545, USA
E-mail: hwang@lanl.gov
Dr. E. F. Holby
Sigma Division
Los Alamos National Laboratory
Los Alamos, NM 87545, USA
Prof. S. Choudhury
Chemical & Materials Engineering
University of Idaho
Moscow, ID 83844, USA
Dr. A. Chen, Dr. L. Adamska, Dr. S. Tretiak
Center of Integrated Nanotechnology (CINT)
Materials Physics and Applications Division
Los Alamos National Laboratory
Los Alamos, NM 87545, USA
T. Sanchez, Dr. S. Iyer
Bioscience Division
Los Alamos National Laboratory
Los Alamos, NM 87545, USA
H. Zhang, L. Zhu, H. Lin, Prof. G. Wu
Department of Chemical and Biological Engineering
University at Buffalo
The State University of New York
Buffalo, NY 14260, USA
E-mail: gangwu@buffalo.edu
Prof. L. Dai
Center of Advanced Science and Engineering for Carbon (Case 4-Carbon)
Department of Macromolecular Science and Engineering
Case Western Reserve University
10900 Euclid Avenue, Cleveland, OH 44106, USA

DOI: 10.1002/adma.201603613

this issue, recent efforts of using inorganic materials to intercalate into graphene sheet to prevent the restacking of graphene have been demonstrated.[12]

To mitigate the cyclic stability issue, it is crucial to develop structurally robust, graphene-based anode materials. Nevertheless, most of the studied graphene anode materials are actually reduced graphene oxide (rGO), which is typically prepared using a complex chemical protocol through harsh oxidation processes.[13] So far, none of the reduction methods reported can completely recover the sp^2 lattice structure from GO.[13,14] Thus, the as-prepared rGO materials have poorly defined molecular structures with many defects, leading to an electron mobility at least two orders of magnitude lower than the theoretical value for defect-free graphene.[13,15] Therefore, heterogeneous rGO materials developed from all of previous studies possess ill-defined molecular structures, which are not suitable for establishing structure–property relationships between the anode materials and energy storage properties in LIBs. Moreover, the performance reproducibility of current rGO anodes remains a great concern due to their poorly controlled structures in those heterogeneous systems.

In this work, we have, for the first time, developed a bottom-up organic synthesis of 3D triarylamine-based nanographenes (NGs) with well-defined molecular structures. Triarylamines have a propeller-shaped structure consist of three flakes and center sp^3-hybridized nitrogen. A variety of functional groups have been covalently attached to the NG flakes to fine-tune electron density on each flake and *d*-spacing between flakes, which provide us with the capability to achieve optimum geometric and electronic structures for efficient Li incorporation/extraction and diffusion.

In addition, the 3D nature of the NG is expected to have a π–π interaction between flakes, capable of yielding a robust self-assembled structure that remains unchanged throughout the long-term charging–discharging cycles. In contrast, the extensive π–π interaction between 2D graphene layers often leads to collapse of interlayer space. Therefore, these 3D NG assemblies are able to overcome the restacking issue observed in traditional rGO sheets, achieved high Li storage capacity and diffusivity, and simultaneously address the long-term stability issues. More importantly, such-synthesized NGs with well-defined molecular and electronic structures can serve as ideal model systems to provide fundamental understanding of correlations among functionalized groups, and resulting electronic property, *d*-spacing, and electrochemical properties for energy storage in LIBs (**Figure 1**a).

The NG, hexabenzocoronenes (HBCs) were synthesized with a multistep solution-chemistry route[16] and schematically outlined in Scheme S1 (Supporting Information). At first, compounds tris[4-(2-phenylethynyl)phenyl)]amine (**Ph_3TPA**) and tris(4-((4-tert-butylphenyl)ethynyl)phenyl)amine (***t*Bu_3TPA**) were synthesized by threefold Sonogashira coupling of the triiodo compound tris(4-iodophenyl)amine (**I_3TPA**) with phenylacetylene and 4-*tert*-butylphenylacetylene, respectively. The hexaphenylbenzenes (HPBs) were achieved by heating **Ph_3TPA** and ***t*Bu_3TPA** with various tetraphenylcyclopentadienones to realize a threefold Diels–Alder reaction and elimination of CO. The as-synthesized HPBs were then planarized (fusion of benzene rings) by treating with $FeCl_3$ in a dichloromethane/nitromethane mixture for 2–3 h to form the corresponding NGs. After quenched the reaction with methanol, repetitive dissolution and precipitation with dichloromethane/methanol yielded NGs as orange to dark red solid powders (Figure 1b). While all of the reaction intermediate HPBs were purified and confirmed with NMR spectroscopy, we were not able to detect the aromatic protons with conventional liquid-phase NMR spectroscopy even at elevated temperatures due to dynamic aggregation of the nanographene HBCs and their high rigidity. **HBC-OMe** is the only exception due to its higher solubility in dimethyl sulfoxide (DMSO). As a result, the HBC structure was determined with matrix assisted laser desorption ionization time-of-flight (MALDI-TOF), which has been the only applicable method for characterization of larger polyaromatic nanostructures. The instrument specifications for the 4800 Plus MALDI-TOF/TOF Analyzer used in positive reflector mode. The instrument calibration spectrum exhibits a calculated resolution at full-width at half-maximum of 17 900 for glu-fibrinopeptide B (1.3 pmol μL^{-1}), m/z 1570.7555. Carbon isotopes C13, C14, C15 are also shown in the high resolution spectrum. All sample data were acquired after calibration of the instruments using similar ionization parameters. Therefore, we have carried out the structural characterization of the intermediates and NGs using MALDI-TOF and Raman spectra. All these spectroscopic results are illustrated in Supporting Information (Figures S1–S20) and are in perfect agreement with the proposed molecular structures, thereby confirming the successful preparation of NGs. Furthermore, the thermal stability of NGs was examined by using thermogravimetric analysis (TGA; Figure S21, Supporting Information). These NGs with various functional groups exhibited excellent thermal stability without significant mass loss up to 300 °C under N_2 atmosphere. The graphitized residue (char yield) of these NGs was more than 60% even at 1000 °C, which is attributed to their high aromatic (graphene-like) content as manifested by their similar Raman spectra (Figure S20, Supporting Information).

Our results show the introduction of functional groups significantly affects the geometry of NGs. The as-synthesized NGs with various functional groups exhibited a change in *d*-spacing between self-assembled flakes. The overall structural stability of NG assemblies is also largely dominated by π–π interaction and the *d*-spacing between flakes as manifested by high-resolution transmission electron microscopy (HRTEM), as shown in **Figure 2**a. Such self-assembled domains are similar to those of graphene nanosheets,[17] indicating a π–π interaction between the neighboring flakes in NGs (Figure 2b). NGs with hydrogen, methoxy, *tert*-butyl, hydroxy, bromo, and fluoro functional groups attached to the flakes have corresponding *d*-spacing of 3.95, 4.08, 4.36, 4.04, 4.30, and 4.0 Å, respectively. The average *d*-spacing around 3.95–4.36 Å for these NGs is much larger than that of the pristine graphite (3.34–3.37 Å)[18] (**Table 1**). It is notable that the *d*-spacing between flakes as determined by TEM is consistent with the size of the functional groups (*t*BuOMe > Br > OMe > OH > F > H), which is also validated by the corresponding X-ray diffraction (XRD) measurements (Figure S22, Supporting Information) and reveal a smaller peak angle with increasing size of the substituents (functional groups).

We use density functional theory (DFT) to understand how these functional groups and their resultant shifts in *d*-spacing

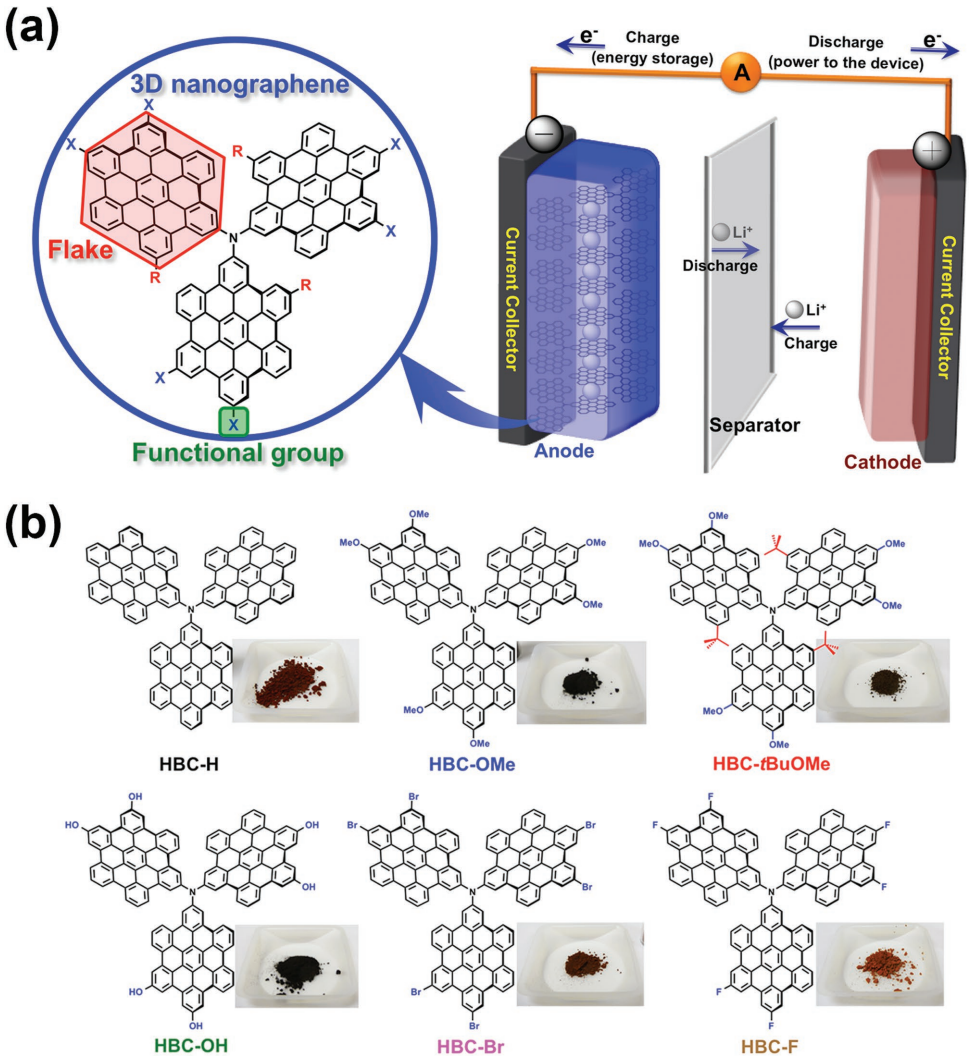

Figure 1. a) Chemical structures of triarylamine-based NG anodes, and the schematic view of LIBs. b) Chemical structures and appearance of triarylamine-based NG powders with various functional groups.

impact the Li binding energy, and hence charge capacity. A series of DFT calculations were carried out to simulate Li binding energy between two AB stacked graphene layers with fixed *d*-spacing. Results of the Li binding energy versus *d*-spacing are shown in Figure 2c and details of the DFT calculation can be found in the Supporting Information. Consistent with the experimental findings, Figure 2c clearly shows that there is a minimum, exothermic Li binding energy at a *d*-spacing of 4.07 Å. Compression of the Li ion between the two layers with a *d*-spacing below 4.07 Å leads to an increase in the system energy. At *d*-spacing values above this minimum, the Li is not stabilized as strongly through chemical interactions with both layers and so the system energy increases. By invoking a previously established descriptor relationship between Li binding and charge capacitance,[19] we believe that NG structures of a *d*-spacing close to 4.07 Å for balanced mechanical and chemical interactions with Li ions have the highest Li charge capacity compared to other graphitic structures. Thus, functional groups can be used to control *d*-spacing and electron density of NG anodes, allowing us to ascertain and optimize Li incorporation and diffusion for maximum battery performance.

We therefore studied these newly developed NGs as anodes in LIBs and determined their Li storage capability. The NG anode performance in terms of their charge capacity and cycle stability was studied as a function of substituent groups on the flakes, which is directly compared to a rGO anode. As shown in **Figure 3**a, the anode **HBC-H** without any functional group exhibited excellent performance durability over 100 charging–discharging cycles and a reversible charging–discharging capacity of 600 mAh g^{-1}. The capacity observed with the anode **HBC-H** (unsubstituted NG) is nearly two times higher than that of a graphite anode. As expected, the rGO anode experienced a more than 50% capacity loss after 100 charging–discharging cycles. In contrast to rGO, the significantly improved battery cyclic stability observed with anode **HBC-H** is likely due to its unique 3D structure with limited flake size, which allows the NG self-assembled into ordered hierarchical structures. The hierarchical self-assembly of **HBC-H** also revealed

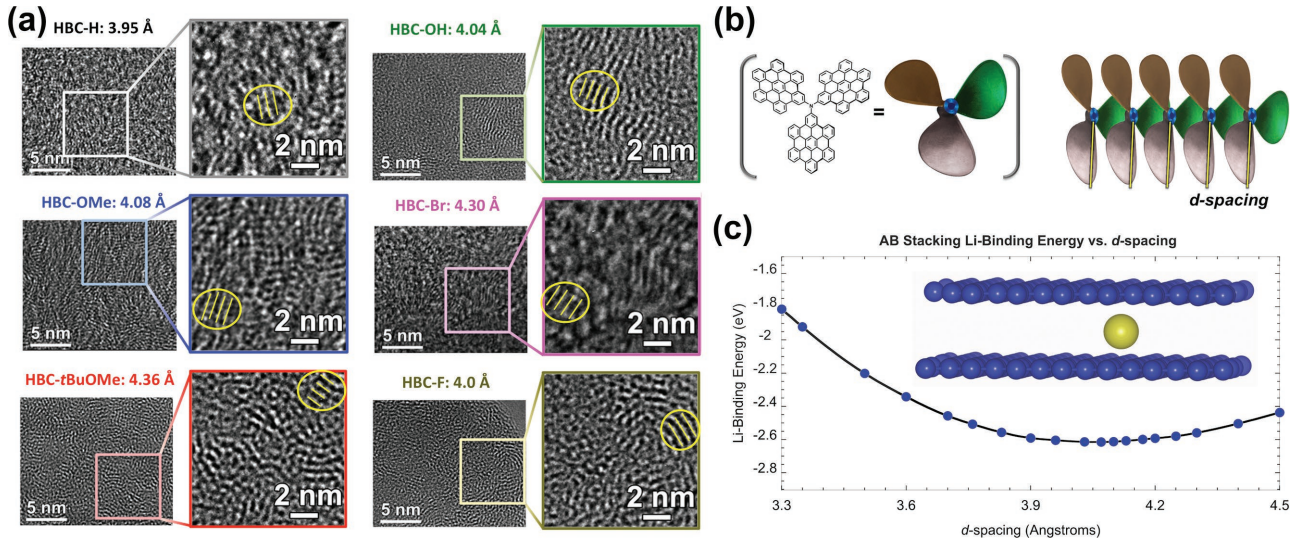

Figure 2. a) TEM images of all six NGs; the *d*-spacing is determined by estimating the distance between the two yellow lines, which is the same as two yellow lines in (b). b) Schematic representation of NG self-assembly into highly ordered structures by stacking one flake on top of another, *d*-spacing between NG flakes is represented as the distance between two blue lines. c) Calculated Li binding energy as a function of fixed *d*-spacing between two AB-stacked graphene layers. The inset is a diagram of the minimum binding energy structure showing *d*-spacing (4.07 Å) and distance between neighboring carbon (blue spheres) and Li (yellow sphere).

that the stacked NGs with only 1 nm in size could easily reach structural equilibrium after a few charging–discharging cycles as compared to conventional rGO that took tens charging–discharging cycles to stabilize (Figure 3a). Note that the initial performance loss is universally observed for anode materials in LIBs due to the formation of solid–electrolyte interface (SEI), which is affected by surface chemistry and crystalline structures and has been discussed in the Supporting Information.[20] It should be noted that all NG anodes have a very stable cyclic performance with 100% coulombic efficiency after initial performance loss, suggesting the SEI films are very dense and able to prevent further decomposition of electrolyte on the NG anodes (Figure S23, Supporting Information). In addition, cyclic voltammograms (CVs) of LIB from various NGs were carried out to better understand the sources of additional capacity. Despite a significantly increased capacity in anode **HBC-H**, its CV during charging–discharging process in a battery exhibits a broad reduction and an oxidation peak around 0.5 V, resemble to that of traditional rGO anode (see Figure S24a, Supporting Information). Their capacities were measured above 0.5 V, attributable to the adsorption of Li ions on the surface or at the edge sites of graphene nanosheets.[6,21]

Table 1. Correlation of *d*-spacing between layers and anode performances of NGs.

	d-spacing [Å]	Charge capacitance [mAh g^{-1}]	
		5th cycle	50th cycle
Graphite	3.35[a)]	377	330
Reduced GO (rGO)	3.59[a)]	735	450
HBC-H	3.95[b)]	625	600
HBC-OMe	4.08[b)]	940	920
HBC-*t*BuOMe	4.36[b)]	830	780
HBC-OH	4.04[b)]	560	510
HBC-Br	4.30[b)]	635	370
HBC-F	4.0[b)]	415	350

[a)]*d*-spacing calculated from X-ray diffraction peaks; [b)]*d*-spacing measured from TEM.

Another important structural factor affecting lithium absorption in layered carbon structure is the *d*-spacing between layers. Lithium can occupy either the available space between the carbon layers (intercalated lithium) or can be deposited as a multilayer on the carbon surface (multilayer lithium) or even interact with functional groups attached to the graphene flaks (oxygen, nitrogen, etc.).[22] In addition, oxygen-containing functional groups (methoxy) directly contribute to the increase in the number of Li incorporation as Li can directly complex with the oxygen atom to form a low energy ionic bond.[1] The effect of functional groups on the battery performance is shown in Figure 3a, including methoxy, *tert*-butyl, hydroxy, bromine, and fluorine. Amongst all NGs, the highest capacity was measured with methoxy-functionalized **HBC-OMe** anode, followed by **HBC-*t*BuOMe > HBC-H > HBC-OH > HBC-Br > HBC-F**.

In addition, Table 1 lists the measured capacity of NGs with respect to the functional groups and *d*-spacings. The increased *d*-spacing from 3.95 (**HBC-H**) to 4.08 Å (**HBC-OMe**) has led to a significant improvement in capacity, from 600 to 950 mAh g^{-1}. Besides structural modification which increases *d*-spacing between NG layers, the oxygen containing functional groups allowing directly complex with Li and electron donating groups stabilize greater number of Li can all contribute to the overall charge capacity. In fact, such high charge capacities are well within the calculated theoretical capacity, as high as 2000 mAh g^{-1} (Supporting Information).[23] However, a further increase in the *d*-spacing (**HBC-*t*BuOMe**) results in a slight decrease of capacity from 950 to 880 mAh g^{-1}, suggesting the optimum *d*-spacing is at ≈4.08 Å. In particular, we compare the capacity of these NGs after 5 and 50 charge–discharge cycles

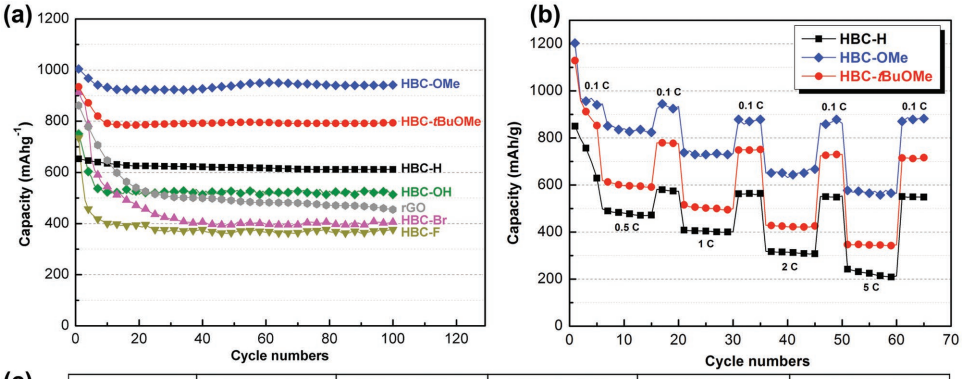

(c)

Polarons in molecules	HBC-H	HBC-OMe	HBC-OH	HBC-Br	HBC-F
IP	5.17	5.23	5.19	5.32	5.27
EA	1.73	1.76	1.74	1.99	1.90
SE(P-*)	0.267	0.261	0.269	0.368	0.342

Figure 3. a) Capacity of NG anodes as a function of charging–discharging cycles. Traditional reduced graphene oxide anode is included to draw comparison between rGO and NGs with various functional groups. b) Rate performance of three most promising **HBC-OMe**, **HBC-*t* BuOMe**, and **HBC-H** NG anodes. c) Orbital plots of electron distribution on a radical anion nanographene flake. SE: stabilization energy of a radical anion nanographene. IP: ionization potential. EA: electron affinity.

to demonstrate their stability. Continuous degradation was found for rGO from 735 (5th cycle) to 450 mAh g^{-1} (50th cycle), resulting in a 38% decrease in capacity. In contrast to rGO, the NG anodes **HBC-OMe**, **HBC-H**, and **HBC-*t*BuOMe** have a reduction of capacity (from 5th cycle to the 50th cycle) of 2.1%, 4.0%, and 6.0%, respectively. Such a small reduction in capacity for these NGs is a strong indication of structural stability of NG assemblies. In fact, the optimized **HBC-OMe** anode has been carried out for a long-term cycling stability test up to 250 charging–discharging cycles, and the charge capacity remains greater than 900 mAh g^{-1}.

The above results suggest that *d*-spacing of NGs resulting from the steric hindrance between attached functional groups plays a critical role in governing Li storage capacity and the newly developed NGs have the potential to be a new class of high-performance anode materials for LIBs. This finding is in strong agreement with that the *d*-spacing of ≈4.08 Å determined by TEM and DFT calculations (Figure 2a,c) for **HBC-OMe** showed the highest Li charge capacity in this study. Noteworthy, there is a clear trend in which electron donating groups (e.g., methoxy **HBC-OMe**, *tert*-butyl methoxy **HBC-*t*BuOMe**) have the higher capacity followed by unsubstituted **HBC-H** and electron withdrawing groups (e.g., bromine, and fluorine) with relatively low capacity. Hydroxyl has a slightly smaller capacity as compare to the unsubtituted NG, presumably due to the intermolecular hydrogen bonding, which can inhibit the Li binding (smaller number of binding sites). This is the first time that a strong correlation between functional group and charging capacity has been elucidated. The rationale behind this trend is because these functional groups can vary the electron density of the NGs that leads to different oxidation/reduction potentials, as determined by CV. These CVs were recorded in acetonitrile containing tetrabutylammonium perchloride as the electrolyte (Figure S24b, Supporting Information). The determined oxidation potentials of NGs follow the order of **HBC-OMe** < **HBC-OH** < **HBC-*t*BuOMe** < **HBC-H** < **HBC-Br** < **HBC-F**. This trend is consistent with our hypothesis that increasing the electron density in NG by attaching electron donating groups (e.g., methoxy **HBC-OMe**, *tert*-butyl methoxy **HBC-*t*BuOMe)** will lead to a smaller oxidation potential. Vice versa, a decrease in electron density in NGs with electron withdrawing groups (e.g., bromine and fluorine) will lead to an increase in oxidation potential. Moreover, increase in electron density on NG can stabilize the Li^+ and decreases the interaction between Li^+ ions. In contrast, the electron withdrawing groups, such as F- and Br-, result in a further decrease in electron density on NGs, which in turn destabilizes the Li^+ and increases unfavorable interaction between Li ions.

Besides specific capacitance and cyclic stability, rate performance of the most promising three NGs (**HBC-OMe**, **HBC-*t*BuOMe**, and **HBC-H**) was also studied. As shown in Figure 3b, the **HBC-OMe** anode demonstrated the best rate performance, capable of maintaining an exceptionally high capacity of 600 mAh g^{-1} at a 5 C charging and discharging rates. Upon decreasing the rate from 5 to 0.1 C, the reversible capacities of the **HBC-OMe** were recovered back to >900 mAh g^{-1}. Thus, in the 3D NG assemblies, the optimal *d*-spacing (**HBC-OMe)** leads to favored Li binding energy and Li diffusion, along with an increased electron density to maximize Li incorporation with excellent rate performance. Our experimental results clearly show that the NG anodes are able to maintain structural stability during the Li insertion/extraction with very high capacity

and high rate performance, which are keys to the development of highly efficient LIBs.

Furthermore, the impact of functional groups on electronic properties of anionic/radical anion NG was further validated by the DFT simulations, which clearly shows a functional group-dependent stabilization energy (SE) defined as vibronic relaxation energy of the negatively charged species to its lowest energy geometry (Figure 3c). Observed trend in the SE can be rationalized by examining the spin density distribution of an extra electron on the molecule. The anion/radical anion NG with electron withdrawing functional group reveals a seriously distorted and localized electron distribution; most of the electrons reside on one side of the flake (Figure 3c). Such configuration forces most of the Li^+ to crowd into one side of the NG flake, limiting the number of Li^+ incorporated into the matrix due to Li–Li repulsion. In contrast, the anion/radical anion with electron donating functional group leads to a homogeneous/uniform electron distribution throughout the flake, which is beneficial for maximizing the number of Li^+ incorporated into the NG. The charging process (Li^+ insertion reaction) in NG anodes requires stabilization of Li^+ and subsequent electron transfer to Li^+. The calculated stabilization energy (i.e., the energy difference in LUMO before and after electron added to NG) of NG radical anion varies from 0.26 (**HBC-OMe**) to 0.37 eV (**HBC-F**), see Figure 3b. A smaller SE means the LUMO electron is in a higher energy state; therefore, it is more easily transferred to Li^+. The magnitude of the SE follows the trend of **HBC-OMe** < **HBC-OH** ~ **HBC-H** < **HBC-F** < **HBC-Br**, which is again consistent with our hypothesis and experimental results. Thus, these simulations have further strengthened our hypothesis that charge capacity is directly associated with the electron donating/withdrawing nature of the functional group.

In summary, we synthesized a series of 3D NGs with a variety of functional groups from hydrogen, methoxyl, *tert*-butyl, hydroxy, bromine, to fluorine through a multistep organic synthesis route using triphenylamine as the starting material. Our studies indicate that the best performing 3D NG anode exhibits a very high capacity (≈950 mAh g^{-1}) almost three times larger than that of the conventional graphite anode (372 mAh g^{-1}) with an excellent stability over 250 charge–discharge cycles. These NGs have relatively small graphene flakes, hence forming a more robust self-assembled hierarchical structures. In addition, maximum electron density on the NGs and optimal *d*-spacing in the 3D NG self-assemblies have led to a significantly enhanced LIB anode charge capacity and cyclic stability. Our results have clearly demonstrated a structure–property correlation between the nature of functional groups and Li storage capacity. More importantly, results obtained from substantial DFT calculations are in good agreement with our electrochemical and battery measurements, identifying the mechanism on how NG electronic and geometric structures dominate the overall battery performance. Such understanding will serve as fundamental principles for the rational design of advanced materials via controlled organic synthesis for efficient energy storage.

Supporting Information

Supporting Information is available from the Wiley Online Library or from the author.

Acknowledgements

The authors would like to acknowledge financial support by the Laboratory Directed Research and Development (LDRD) program (E.F.H., S.C., G.W. and H.-L.W.) at Los Alamos National Laboratory (LANL). H.-J.Y. thanks the J. R. Oppenheimer Fellowship for supporting the synthesis of NGs and lithium-ion batteries fabrication. S.T. acknowledges the LANL Institutional Computing (IC) Program provided computational resources. G.W. is grateful the start-up fund from the University at Buffalo, SUNY along with National Science Foundation (CBET-1511528).

Received: July 8, 2016
Revised: August 25, 2016
Published online: October 10, 2016

[1] a) C. K. Chan, H. Peng, G. Liu, K. McIlwrath, X. F. Zhang, R. A. Huggins, Y. Cui, *Nat. Nanotechnol.* **2008**, *3*, 31; b) N. A. Kaskhedikar, J. Maier, *Adv. Mater.* **2009**, *21*, 2664; c) L.-F. Cui, Y. Yang, C.-M. Hsu, Y. Cui, *Nano Lett.* **2009**, *9*, 3370; d) H. Wang, L.-F. Cui, Y. Yang, H. Sanchez Casalongue, J. T. Robinson, Y. Liang, Y. Cui, H. Dai, *J. Am. Chem. Soc.* **2010**, *132*, 13978; e) P. Lian, X. Zhu, S. Liang, Z. Li, W. Yang, H. Wang, *Electrochim. Acta* **2010**, *55*, 3909; f) Z. Fan, J. Yan, G. Ning, T. Wei, L. Zhi, F. Wei, *Carbon* **2013**, *60*, 558; g) Z.-L. Wang, D. Xu, H.-G. Wang, Z. Wu, X.-B. Zhang, *ACS Nano* **2013**, *7*, 2422; h) R. Mukherjee, A. V. Thomas, D. Datta, E. Singh, J. Li, O. Eksik, V. B. Shenoy, N. Koratkar, *Nat. Commun.* **2014**, *5*, 3710; i) S. Goriparti, E. Miele, F. De Angelis, E. Di Fabrizio, R. Proietti Zaccaria, C. Capiglia, *J. Power Sources* **2014**, *257*, 421; j) J. Hou, C. Cao, F. Idrees, X. Ma, *ACS Nano* **2015**, *9*, 2556.

[2] X. Su, Q. Wu, J. Li, X. Xiao, A. Lott, W. Lu, B. W. Sheldon, J. Wu, *Adv. Energy Mater.* **2014**, *4*, 1300882.

[3] A. S. Arico, P. Bruce, B. Scrosati, J.-M. Tarascon, W. van Schalkwijk, *Nat. Mater.* **2005**, *4*, 366.

[4] a) K. S. Novoselov, V. I. Falko, L. Colombo, P. R. Gellert, M. G. Schwab, K. Kim, *Nature* **2012**, *490*, 192; b) Y. Fang, Y. Lv, R. Che, H. Wu, X. Zhang, D. Gu, G. Zheng, D. Zhao, *J. Am. Chem. Soc.* **2013**, *135*, 1524; c) I.-Y. Jeon, M. J. Ju, J. Xu, H.-J. Choi, J.-M. Seo, M.-J. Kim, I. T. Choi, H. M. Kim, J. C. Kim, J.-J. Lee, H. K. Liu, H. K. Kim, S. Dou, L. Dai, J.-B. Baek, *Adv. Funct. Mater.* **2015**, *25*, 1170; d) R. Raccichini, A. Varzi, S. Passerini, B. Scrosati, *Nat. Mater.* **2015**, *14*, 271; e) F. Bonaccorso, L. Colombo, G. Yu, M. Stoller, V. Tozzini, A. C. Ferrari, R. S. Ruoff, V. Pellegrini, *Science* **2015**, *347*, 1246501.

[5] D. Bar-Tow, E. Peled, L. Burstein, *J. Electrochem. Soc.* **1999**, *146*, 824.

[6] E. Yoo, J. Kim, E. Hosono, H.-S. Zhou, T. Kudo, I. Honma, *Nano Lett.* **2008**, *8*, 2277.

[7] D. Pan, S. Wang, B. Zhao, M. Wu, H. Zhang, Y. Wang, Z. Jiao, *Chem. Mater.* **2009**, *21*, 3136.

[8] Z.-S. Wu, W. Ren, L. Xu, F. Li, H.-M. Cheng, *ACS Nano* **2011**, *5*, 5463.

[9] X. Ma, G. Ning, C. Qi, C. Xu, J. Gao, *ACS Appl. Mater. Interfaces* **2014**, *6*, 14415.

[10] H. R. Byon, B. M. Gallant, S. W. Lee, Y. Shao-Horn, *Adv. Funct. Mater.* **2013**, *23*, 1037.

[11] a) Z.-S. Wu, W. Ren, L. Wen, L. Gao, J. Zhao, Z. Chen, G. Zhou, F. Li, H.-M. Cheng, *ACS Nano* **2010**, *4*, 3187; b) A. Magasinski, P. Dixon, B. Hertzberg, A. Kvit, J. Ayala, G. Yushin, *Nat. Mater.* **2010**, *9*, 353; c) X. Zhu, Y. Zhu, S. Murali, M. D. Stoller, R. S. Ruoff, *ACS Nano* **2011**, *5*, 3333.

[12] a) L. Chen, G. Zhou, Z. Liu, X. Ma, J. Chen, Z. Zhang, X. Ma, F. Li, H.-M. Cheng, W. Ren, *Adv. Mater.* **2016**, *28*, 510; b) Z.-S. Wu,

G. Zhou, L.-C. Yin, W. Ren, F. Li, H.-M. Cheng, *Nano Energy* **2012**, *1*, 107.
[13] W. Gao, L. B. Alemany, L. Ci, P. M. Ajayan, *Nat. Chem.* **2009**, *1*, 403.
[14] S. Park, R. S. Ruoff, *Nat. Nanotechnol.* **2009**, *4*, 217.
[15] G. Eda, G. Fanchini, M. Chhowalla, *Nat. Nanotechnol.* **2008**, *3*, 270.
[16] a) W. Pisula, X. Feng, K. Müllen, *Chem. Mater.* **2011**, *23*, 554; b) M. G. Schwab, A. Narita, Y. Hernandez, T. Balandina, K. S. Mali, S. De Feyter, X. Feng, K. Müllen, *J. Am. Chem. Soc.* **2012**, *134*, 18169.
[17] W. Ahn, H. S. Song, S.-H. Park, K.-B. Kim, K.-H. Shin, S. N. Lim, S.-H. Yeon, *Electrochim. Acta* **2014**, *132*, 172.
[18] I.-Y. Jeon, H.-J. Choi, S.-Y. Bae, D. W. Chang, J.-B. Baek, *J. Mater. Chem.* **2011**, *21*, 7820.
[19] Y. Liu, Y. M. Wang, B. I. Yakobson, B. C. Wood, *Phys. Rev. Lett.* **2014**, *113*, 028304.
[20] a) P. Verma, P. Maire, P. Novák, *Electrochim. Acta* **2010**, *55*, 6332; b) K. W. Schroder, H. Celio, L. J. Webb, K. J. Stevenson, *J. Phys. Chem. C* **2012**, *116*, 19737.
[21] Y. Liu, V. I. Artyukhov, M. Liu, A. R. Harutyunyan, B. I. Yakobson, *J. Phys. Chem. Lett.* **2013**, *4*, 1737.
[22] a) R. Yazami, M. Deschamps, *J. Power Sources* **1995**, *54*, 411; b) D.-W. Wang, C. Sun, G. Zhou, F. Li, L. Wen, B. C. Donose, G. Q. Lu, H.-M. Cheng, I. R. Gentle, *J. Mater. Chem. A* **2013**, *1*, 3607.
[23] G. Wang, X. Shen, J. Yao, J. Park, *Carbon* **2009**, *47*, 2049.